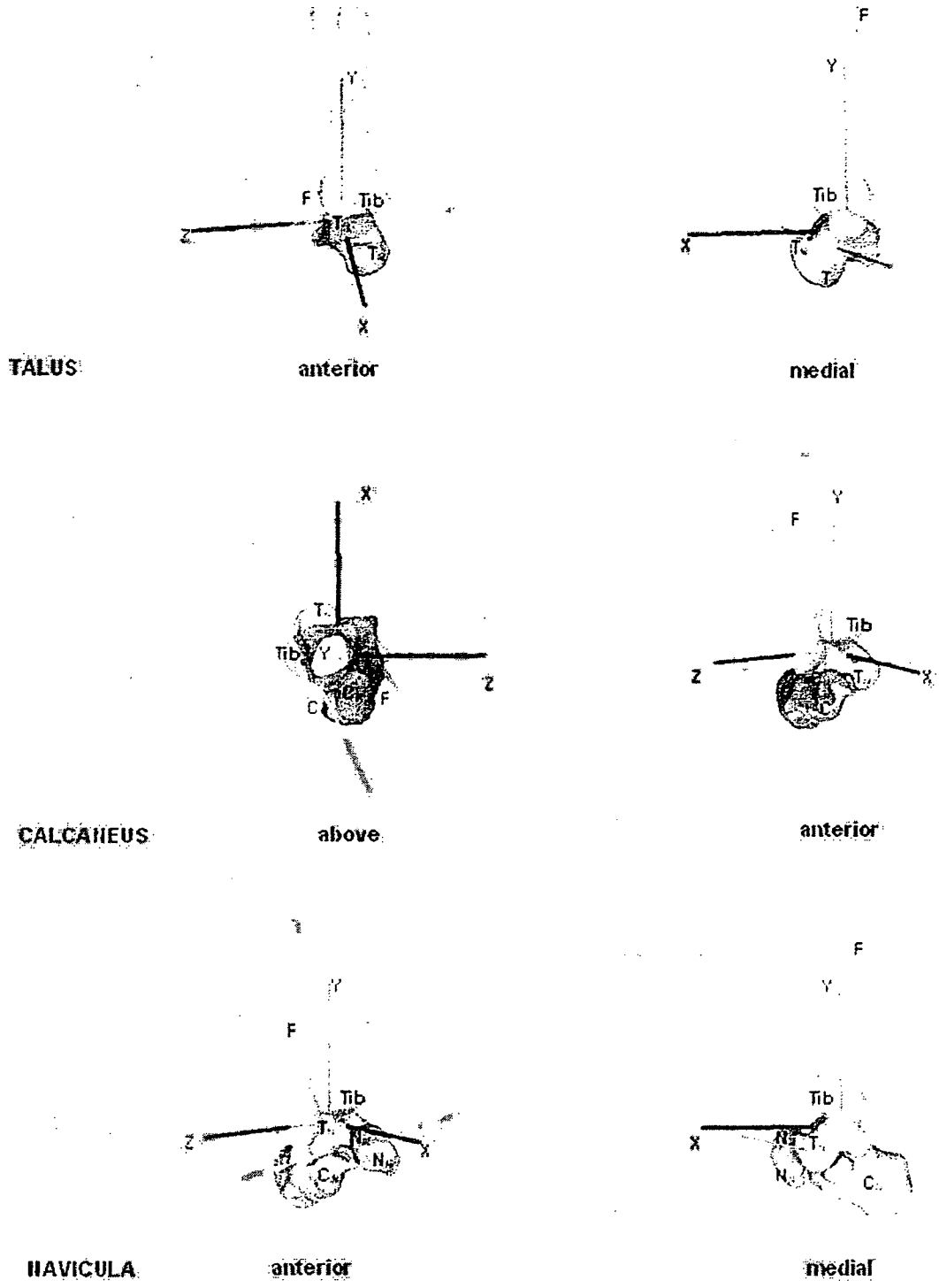

Figure 3. Displacements of the talus, calcaneus, and navicular bones. Tib, tibia; F, fibula; T_N, normal talus; T_R, RA talus; C_N, normal calcaneus; C_R, RA calcaneus; N_N, normal navicular; N_R, RA navicular; X, Y, and Z stand for the *x*-, *y*-, and *z*-axes of the standard coordinate system.

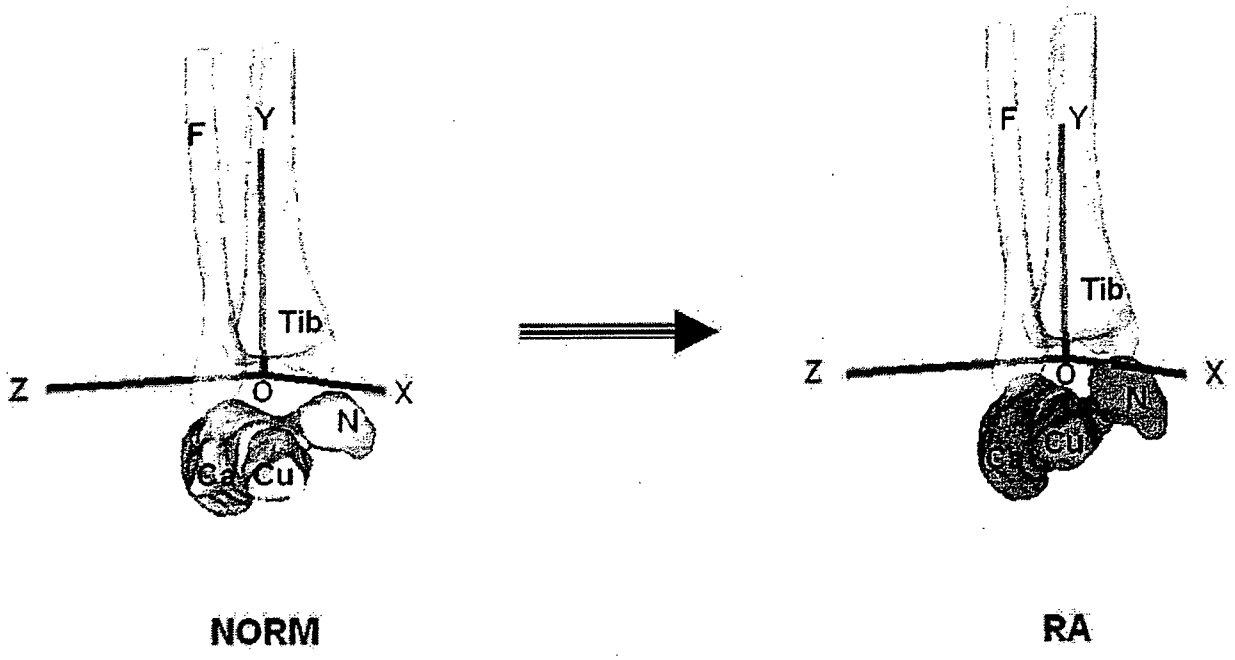

Figure 4. The calcaneus, cuboid, and navicular bones move in the same way. Tib, tibia; F, fibula; Ca, calcaneus; Cu, cuboid; N, navicular; O, origin; X, Y, and Z stand for the *x*-, *y*-, and *z*-axes of the standard coordinate system.

change in the naviculocuneiform joint is recommended.

The relationships among the cuboid, calcaneus, and navicular bones, reported here for the first time, might be helpful in surgical treatment of RA hindfoot valgus deformity. The cuboid showed no displacement relative to the calcaneus, and the navicular had no relative displacement to the cuboid, suggesting that the calcaneus, the cuboid, and the navicular might move in the same pattern. This is supported by findings that the hindfoot valgus deformity in RA patients primarily occurred in the subtalar and talonavicular joints.[4,24] The result might be useful for surgical treatment, because it suggests that in some circumstances, cuboid correction is unnecessary. Double arthrodesis (of the subtalar and talonavicular joints) rather than triple arthrodesis should be more often recommended for patients with RA hindfoot valgus deformity.

Our study is limited by the age mismatch between the patients with RA and the controls. On the other hand, our study was designed to compare the feet deformed by RA with normal feet. Many older people have normal feet, but they may have other deformities caused by OA or diseases such as flat foot, which sometimes is asymptomatic. These conditions make those older people unsuitable as controls. Conversely, not all young people have normal skeletal alignments. However, most young people are suitable as controls. We could not perform CT scans on normal subjects because of the radiation issue. CT resolution for bone is superior to that of MRI. During segmentation, the marching cubes algorithm worked better with CT than with MRI bone margins. However, we believe that ample information is retained using MRI, if geometric properties of a normal bone are desired, such as the calculated geometric centroid and principle axes. In this respect, MRI appears comparable to CT. The difference in accuracy between the MRI and CT groups was very small by validation. Functional CT and MRI of the foot under body-weight loading are desirable, but difficult to achieve.

ACKNOWLEDGMENTS

H. B. Liu was a research fellow sponsored by the Japan–China Medical Association. This work was supported by a Japan–China Sasagawa Medical Scholarship. The authors thank Hisao Moritomo, Guixing Qiu, Wataru Sahara, Kunihiro Oka, Takahiro Ishii, Ryutaro Fujii, Akira Goto, and Ryoji Nakao for their invaluable contributions to the experimental procedure.

REFERENCES

1. Bouysset M, Bonvoison B, Lejeune E, et al. 1987. Flattening of the rheumatoid foot in tarsal arthritis on X-ray. Scand J Rheumatol 16:127–133.

DOI 10.1002/jor

2. Bouysset M, Tebib JG, Weil G, et al. 1987. Deformation of the adult rheumatoid rearfoot: a radiographic study. Clin Rheumatol 6:539–544.
3. Michelson J, Easley M, Wigley FM, et al. 1994. Foot and ankle problems in rheumatoid arthritis. Foot Ankle Int 15: 608–613
4. Spiegel TM, Spiegel JS. 1982. Rheumatoid arthritis in the foot and ankle — diagnosis, pathology, and treatment: the relationship between foot and ankle deformity and disease duration in 50 patients. Foot Ankle 2:318–324.
5. Woodburn J, Udupa KJ, Hirsch BE, et al. 2002. The geometric architecture of the subtalar and midtarsal joints in rheumatoid arthritis based on magnetic resonance imaging. Arthritis Rheum 46:3168–3177.
6. Vahvanen VA. 1967. Rheumatoid arthritis in the pantalar joints: a follow-up study of triple arthrodesis on 292 adult feet. Acta Orthop Scand Suppl 112–119.
7. Keenan MA, Peabody TD, Gronley JK, et al. 1991. Valgus deformities of the feet and characteristics of gait in patients who have rheumatoid arthritis. J Bone Joint Surg Am 73:237–247.
8. Seltzer SE, Weissman BN, Braunstein EM, et al. 1985. Computed tomography of the hindfoot with rheumatoid arthritis. Arthritis Rheum 28:1234–1242.
9. Montagne J, Chevrot A, Galmiche JM. 1981. Atlas of foot radiology. New York: Masson Publishing USA.
10. Saltzman CL, Brandser EA, Berbaum KS, et al. 1994. Reliability of standard foot radiographic measurements. Foot Ankle Int 15:661–665.
11. Seltzer SE, Weissman BN, Braunstein EM, et al. 1984. Computed tomography of the hindfoot. J Comput Assist Tomogr 8:488–497.
12. Ishii T, Mukai Y, Hosono N, et al. 2004. Kinematics of the upper cervical spine in rotation: in vivo three-dimensional analysis. Spine 29:E139–E144.
13. Ishii T, Mukai Y, Hosono N, et al. 2004. Kinematics of the subaxial cervical spine in rotation: in vivo three-dimensional analysis. Spine 29:2826–2831.
14. Goto A, Moritomo H, Murase T, et al. 2005. In vivo three-dimensional wrist motion analysis using magnetic resonance imaging and volume-based registration. J Orthop Res 23:750–756.
15. Moritomo H, Goto A, Sato Y, et al. 2003. The triquetrum-hamate joint: an anatomic and in vivo three-dimensional kinematic study. J Hand Surg (Am) 28:797–805.
16. Itohara T, Sugamoto K, Shimizu N, et al. 2005. Assessment of the three-dimensional relationship of the ossific nuclei and cartilaginous anlagen in congenital clubfoot by 3-D MRI. J Orthop Res 23:1160–1164.
17. Lorensen WE, Cline HE. 1987. Marching cubes: a high resolution 3D surface construction algorithm. Comput Graphics 21:163–169.
18. Cappozzo A, Catani F, Croce UD, et al. 1995. Position and orientation in space of bones during movement: anatomical frame definition and determination. Clin Biomech 10:171–178.
19. Hirsch BE, Udupa JK, Samarasekera, S. 1996. New method of studying joint kinematics from three-dimensional reconstructions of MRI data. J Am Podiatric Med Assoc 86:4–15.
20. Stindel E, Udupa JK, Hirsch BE, et al. 2001. An in vivo analysis of the motion of the peritalar joint complex based on MR imaging. IEEE Trans Biomed Eng 48:236–247.
21. Vainio K. 1956. The rheumatoid foot: a clinical study with pathological and roentgenological comments. Ann Chir Gynec 45(Suppl 1):1–107.
22. Gross MT. 1995. Lower quarter screening for skeletal malalignment — suggestions for orthotics and shoewear. J Orthop Sports Phys Ther 21:389–405.
23. Picciano AM, Rowlands MS, Worrell T. 1993. Reliability of open and closed kinetic chain subtalar joint neutral positions and navicular drop test. J Orthop Sports Phys Ther 18:553–558.
24. Cimino WG, O'Malley MJ. 1998. Rheumatoid arthritis of the ankle and hindfoot. Orthop Clin North Am 24:157–172.

Clin Rheumatol (2007) 26: 515–519
DOI 10.1007/s10067-006-0318-y

ORIGINAL ARTICLE

Takashi Kitamura · Jun Hashimoto · Tsuyoshi Murase · Tetsuya Tomita · Takako Hattori · Hideki Yoshikawa · Kazuomi Sugamoto

Radiographic study of joint destruction patterns in the rheumatoid elbow

Received: 7 January 2006 / Revised: 1 April 2006 / Accepted: 3 April 2006 / Published online: 3 May 2006

Abstract Knowledge of the pattern of joint destruction is important for planning the therapeutic approach to rheumatoid arthritis (RA) of the elbow. Accordingly, we carried out a large-scale radiographic study with the objective of elucidating the joint destruction pattern in rheumatoid elbows. From 2001 through 2003, we examined and took plain X-rays of both elbows of 193 RA patients (i.e., 386 elbows), consisting of 18 men and 175 women, with a mean age of 57.0 years. Radiographic images of the elbow joints were used to classify the degree of bone loss in various zones on the elbow joint surface into four grades of severity, and joint destruction was compared between the left and right elbows. In addition, correlation in the extent of bone loss between each of the zones of the same elbow and differences in the extent of bone loss were analyzed statistically. The results showed direct correlations for destruction of the elbow joint surface among the zones for the left and right elbow joints and in the same elbow joint. However, more severe destruction was observed on the radial side of the humeral trochlea, and it was surmised that destruction of the elbow joint must begin at that site and gradually spread mediolaterally. In addition, in the same elbow joint, the correlation in the degree of bone loss between the trochlea of humerus and the trochlear notch was especially strong, indicating that the bone destruction at both sites represented mirror lesions. We conclude that when performing radiographic diagnosis of the joint damage in the rheumatoid elbow, knowledge of this pattern of joint destruction will be useful for assessing whether there is joint destruction in the initial stage and for deciding the therapeutic approach.

Keywords Elbow joint · Radiography · Rheumatoid arthritis

T. Kitamura (✉)
Department of Orthopedic Surgery, Kaizuka City Hospital,
3-10-20, Hori, Kaizuka,
Osaka 597-0015, Japan
e-mail: kitamura@tb3.so-net.ne.jp
Tel.: +81-0724-225865
Fax: +81-0724-396061

J. Hashimoto · T. Murase · T. Tomita ·
H. Yoshikawa · K. Sugamoto
Department of Orthopaedics,
Osaka University Medical School,
2-2, Yamadaoka, Suita,
Osaka 565-0871, Japan

T. Hattori
Department of Orthopedic Surgery, NTT West Osaka Hospital,
2-6-40,Karasugatsuji,Tennouji,
Osaka 543-8922, Japan

Introduction

The elbow joint is a common site for the development of rheumatoid arthritis (RA), and it is one of the most important joints in the upper limb as it controls the reach of the hand [1–4]. For this reason, disorders of the elbow joint can seriously interfere with activities of daily living (ADL) of RA patients. In general, when arthropathy is mild, therapy consists of conservative treatments such as drug administration and/or intraarticular injection of steroid. In severe disease, surgical treatments such as synovectomy and artificial elbow joint replacement may be performed [1–4]. For treatment selection and planning, it is very important for the physician to have a good understanding of the pattern of destruction that has occurred in the RA elbow joint. However, it is unfortunate that to date very few reports of analysis of the pattern of bone destruction in RA elbow joints have been published.

We therefore carried out a large-scale radiographic study with the objective of elucidating the pattern of RA elbow joint bone destruction.

Subjects

From 2001 to 2003, we examined plain X-rays of both elbow joints of 233 patients who satisfied the ARA diagnostic criteria. Forty of these patients were excluded from the present study due to previous synovectomy or

artificial elbow joint replacement (33 patients) or because the X-rays were unreadable (seven patients). The remaining 193 RA patients, i.e., 386 elbows, were the subjects of this study. They consisted of 18 men and 175 women, with an age range of 23~84 years (mean 57.0 years). History of drug administration, including steroids, and duration of RA were unclear.

Methods

Radiographic classification of the severity of RA was performed on the basis of plain X-ray anteroposterior images and lateral images of the bilateral elbow joints that were obtained for each patient at the time of final examination. X-rays were taken with the patient in a sitting position. Frontal views were obtained with the elbow joint extended and the forearm in the supine position, while lateral views were obtained with the elbow joint flexed at 90° and the forearm in the intermediate position. The frontal images were divided into three zones: the capitulum of the humerus (zone A), the radial side of the humeral trochlea (zone B), and the ulnar side of the humeral trochlea (zone C). The extent of destruction of the joint surface was determined for each of these zones. In addition, from the lateral view, the extent of joint surface destruction was determined for the olecranon (zone D).

Extent of joint destruction was assessed by reference to a template of the normal elbow joint that had been prepared in advance. The ratings used were grade 0, no bone loss; grade 1, less than 3 mm of bone loss from the joint surface; grade 2, bone loss of 3 to less than 6 mm; and grade 3, bone loss of 6 or more mm (Figs. 1 and 2).

We investigated the extent of bone destruction observed in each of the joint zones, and also investigated whether there was any correlation in destruction among the zones. In practice, we first investigated the correlation in the extent of bone loss in the same zone in both elbows of the same patient, and then compared joint destruction in the left and right elbows. In addition, the correlation in the extent of bone loss among each zone of the same elbow and differences in the extent of bone loss were analyzed statistically.

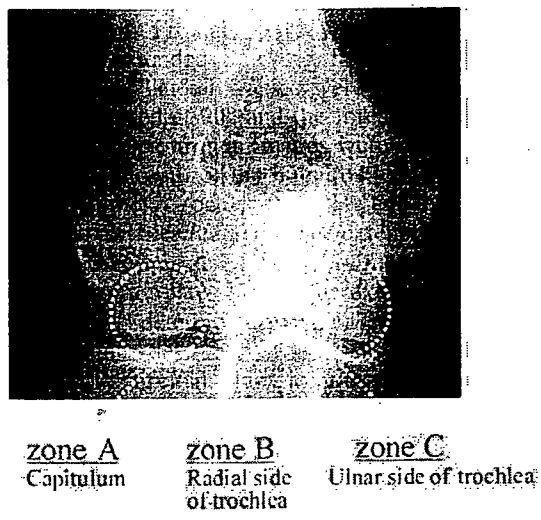

Fig. 1 Radiographic classification (*zones A, B,* and *C*)

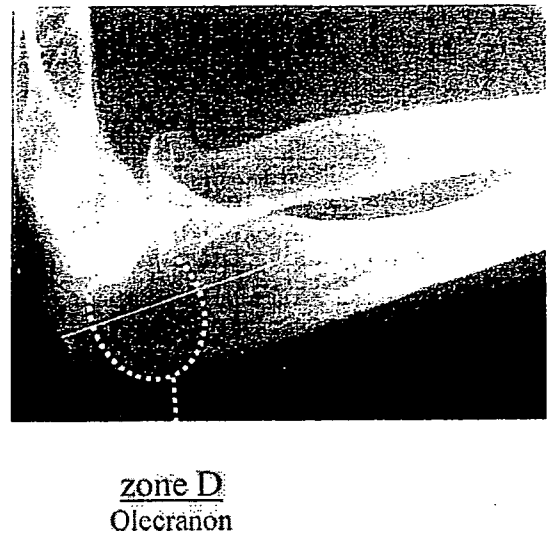

Fig. 2 Radiographic classification (*zone D*)

Spearman's ranked correlation coefficients were used for statistical analyses of correlations, while one-way analysis of variance (ANOVA) and Fisher's least significant difference (LSD) test were used to analyze differences in extent of bone loss.

Results

The extent of bone loss in each zone of the joint as seen on frontal X-ray images was as follows: zone A, 26.2% grade 0, 62.1% grade 1, 8.8% grade 2, and 2.8% grade 3; zone B, 26.2% grade 0, 37.0% grade 1, 26.9% grade 2, and 9.8% grade 3; and zone C, 26.9% grade 0, 62.1% grade 1, 2.6% grade 2, and 8.3% grade 3. The extent of bone loss was therefore similar in zone A and zone C, whereas zone B exhibited a lower percentage rated as grade 2 and a higher percentage rated as grade 3 compared with the other two zones. The extent of bone loss seen on lateral X-ray images (zone D) was grade 0 in 27.2%, grade 1 in 61.1%, grade 2 in 8.3%, and grade 3 in 3.4% (Table 1).

A significant correlation was found for the extent of bone loss in the same zone between the left and right elbows, and correlation was found for bilateral elbow joint destruction (zone A r=0.833, p<0.001; zone B r=0.804, p<0.001; zone C r=0.881, p<0.001; and zone D r=0.887, p<0.001).

In addition, statistically significant correlations were also found for the extent of bone loss among zones in the same elbow (r=0.789~0.951, p<0.001) (Fig. 3). A particularly strong correlation was demonstrated between zone C and zone D (r=0.951, p<0.001).

On the other hand, the extent of bone loss was significantly greater in zone B compared with zone A and zone C (p<0.05), indicating that joint surface

Table 1 Radiographic classification of severity of joint destruction in the elbow (n=193)

Grade	Zone A		Zone B		Zone C		Zone D	
	R/L	Total(%)	R/L	Total(%)	R/L	Total(%)	R/L	Total(%)
0	50/51	26.2	49/52	26.2	51/53	26.9	51/54	27.2
1	123/117	62.2	73/70	37.1	120/120	62.2	117/119	61.1
2	14/20	8.8	54/50	26.9	7/3	2.6	16/16	8.3
3	6/5	2.8	17/21	9.8	15/17	8.3	9/4	3.4
Total	193/193	100	193/193	100	193/193	100	193/193	100

destruction was more advanced in the central part of distal humerus articular surface than at other sites (Fig. 4).

In addition, bone destruction of the humeral trochlea that extended to the olecranon fossa, i.e., a so-called Y-shaped

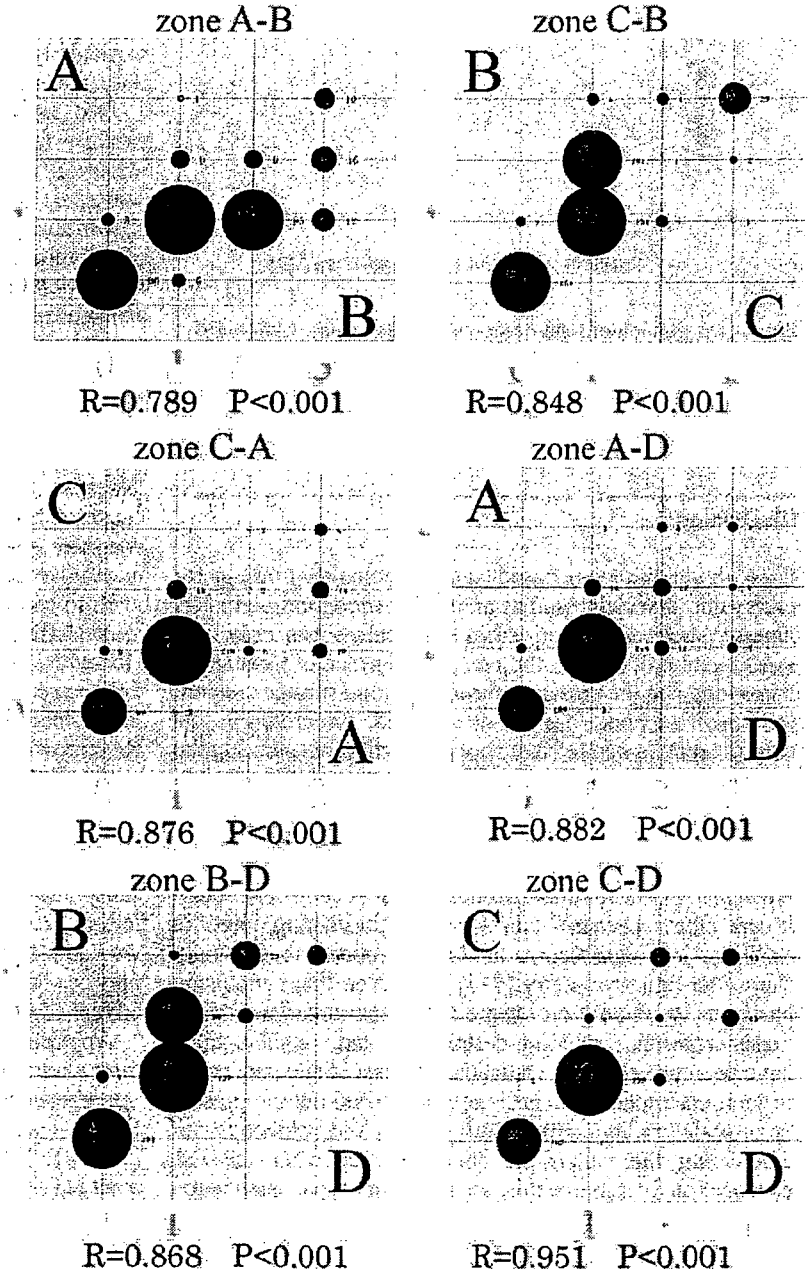

Fig. 3 Correlation of joint destruction among *zonesA*, *B*, *C*, and *D* (386 joints)

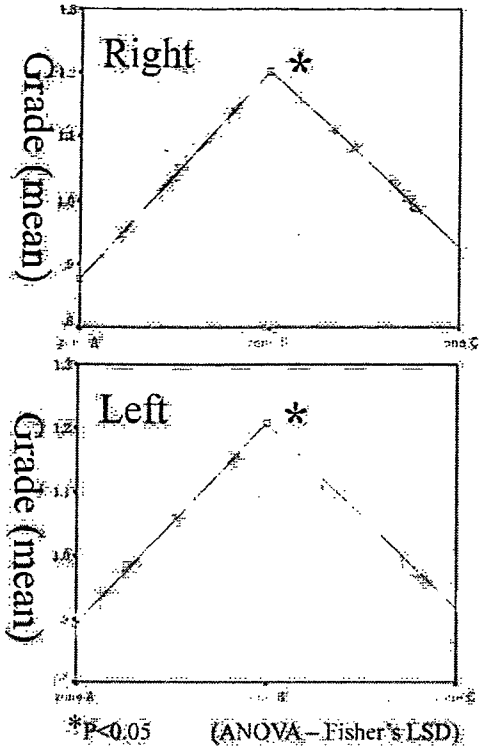

Fig. 4 Distribution of joint destruction grade (*zones A, B,* and *C*)

deformity, was observed in six of the patients, although this was bilateral in only two patients.

Discussion

Larsen's classification, based on the radiological findings for each joint, is widely used as an index of progression of RA disease stage. However, this classification has only two assessment criteria, i.e., the presence/absence of joint space narrowing and the presence/absence of joint surface erosion; the extent of bone loss is not assessed. Accordingly, this classification is said to have poor sensitivity for assessing the extent of joint destruction [5–7]. Lehtinen et al. [7] reported that joint space narrowing in the RA elbow differs from that in weight-bearing joints in that it occurs only subsequent to erosive destruction. They also stated that caution is necessary when using Larsen's classification to assess bone destruction in the elbow because it is a nonweight-bearing joint. In addition, joint destruction in RA is reported to generally show left–right symmetry [5–7]. However, that conclusion has been based only on simple bilateral comparison of the presence/absence of joint destruction, and, to date, there have been no reports of statistical analysis of site and extent of joint destruction. Accordingly, we carried out the present large-scale radiographic study with the objective of elucidating the pattern of bone destruction in the RA elbow joint. To achieve this, we used our own classification system to assess the extent of bone loss in various zones on the elbow joint surface, and joint destruction was compared between the left and right elbows. We then performed statistical analyses to determine whether there were any correlations in the extent of bone loss among each of the zones in the bilateral elbows and in the same elbow.

Our patients showed positive correlations among each of the zones for the extent of bone loss in the same elbow joint, and positive correlations were also found for the extent of joint surface bone loss in the same zones in the bilateral elbows. On the other hand, when we investigated the extent of bone loss in each zone in the same joint, we found it to be significantly greater on the radial side of the humeral trochlea compared with the ulnar side of the trochlea and the capitulum. We therefore surmised that the joint destruction must begin at the radial side of the humeral trochlea and gradually spread mediolaterally. In addition, in the same elbow joint, the correlation in the degree of bone loss between the ulnar side of the trochlea and the olecranon was particularly strong, indicating that the bone destruction at both sites represented symmetrical lesions.

Two theories have been proposed in an attempt to explain the underlying mechanism of the destruction observed in upper limb joints with RA. In the first, the principal cause is considered to be destruction and absorption of cartilage and bone as a result of the actions of cytokines released from the synovial tissue [8, 9]. The second theory holds that the major effects arise from anatomical and/or mechanical factors [10]. Ochi et al. [11] reported that even in the same joint the mechanism of destruction varies widely depending on the disease type. That is, they found that in the type involving damage to the smaller joints, the main bone destruction consisted of erosion of the joint surface due to proliferation of synovitis. Whereas with the mutilating type of arthritis, the main cause of bone destruction was crushing of bone that had become highly osteoporotic because of severe joint instability due to joint laxity.

It is possible that the level of stress applied to the elbow joints differs between the dominant and nondominant arm. However, in the present study, we found no clear left–right difference in the extent of joint destruction, suggesting that the effects of mechanical factors on bone destruction in the RA elbow are slight. Even so, consideration must be given to the fact that most of the patients in our present series were at an earlier stage of the disease, showing a milder degree of joint destruction. Conversely, however, some patients with severe joint destruction, such as is likely to cause the so-called Y-shaped deformity, exhibited clear left–right differences in the extent of damage. Therefore, we cannot rule out the possibility that mechanical factors play a larger role than immunological factors in the advanced stages of joint destruction.

Application of axial compression in the direction of the long axis of the forearm reportedly results in almost equal transmission of the force to the radial joint and the ulnar joint, or slightly greater transmission to the radial joint [12–14]. The surface of the radial side of the humeral trochlea becomes the varus–valgus pivot point of the elbow [15], and for this reason it is possible that when joint laxity occurs due to synovitis, forces are concen-

trated in that area and this leads to the progression of joint destruction.

Our present results indicated the possibility that joint destruction in the RA elbow begins on the radial side of the humeral trochlea and gradually spreads mediolaterally. If we accept the validity of this pattern of destruction of the elbow joint, then when analyzing X-rays taken in the early stage of RA elbow joint damage, it should be possible to focus on the radial side of the humeral trochlea and determine whether joint destruction had already begun. In addition, if bone destruction on the radial side of the trochlea were mild, we would be able to conclude that the joint destruction was at an early stage and that a minimally invasive therapy such as synovectomy was indicated.

The progression of joint destruction can be considered influenced by various factors, such as medication (including NSAIDs, DMARDs, and steroids), disease duration, and progression of joint deformation due to aging or osteoporosis [16–19]. A limitation of the present study was that we were unable to discuss the possible effects of drug treatments, disease duration, and aging in our patient series. However, this is the first report of a statistical analysis of the pattern of joint destruction in the rheumatoid elbow, and we think that our findings will make a significant contribution to decision making regarding therapeutic approaches to RA of the elbow.

References

1. Boyd AD, Thornhill TS (1989) Surgical treatment of the elbow in rheumatoid arthritis. Hand Clin 5(4):645–655
2. Rosenberg GM, Tuner RH (1984) Nonconstrained total elbow arthroplasty. Clin Orthop 187:154–162
3. Linclau LA, Winia WPCA, Korst JK (1983) Synovectomy of the elbow in rheumatoid arthritis. Acta Orthop Scand 54 (6):935–937
4. Pritchard RW (1991) Total elbow joint arthroplasty in patients with rheumatoid arthritis. Semin Arthritis Rheum 21(1):24–29
5. Ljung P, Jonsson K, Rydgren L, Rydholm U (1995) The natural course of rheumatoid elbow arthritis: a radiographic and clinical five-year follow up. J Orthop Rheumatol 8:32–36
6. Lehtinen JT, Kaarela K, Kauppi MJ, Belt EA, Maenpaa HM, Lehto MUK (2002) Bone destruction patterns of the rheumatoid elbow: a radiographic assessment of 148 elbows at 15 years. J Shoulder Elbow Surg 11:253–258
7. Lehtinen JT, Kaarela K, Belt EA, Kauppi MJ, Skytta E, Kuusela PP, Kautiainen HJ, Lehto MUK (2001) Radiographic joint space in rheumatoid elbow joints. A 15-year prospective follow-up study in 74 patients. Rheumatology 40:1141–1145
8. Kirwan JR (1997) The relationship between synovitis and erosions in rheumatoid arthritis. Br J Rheumatol 36:225–228
9. Cuomo F, Greller MJ, Zuckerman JD (1998) The rheumatoid shoulder. Rheum Dis Clin North Am 24:67–82
10. Tan AL, Tanner SF, Conaghan PG, Radjenovic A, O'Connor P, Brown AK, Emery P, McGonagle D (2003) Role of metacarpophalangeal joint anatomic factors in the distribution of synovitis and bone erosion in early rheumatoid arthritis. Arthritis Rheum 48:1214–1222
11. Ochi T, Iwase R, Yonemasu K, Matsukawa M, Yoneda M, Yukioka M, Ono K (1988) Natural course of joint destruction and fluctuation of serum C1q levels in patients with arthritis. Arthritis Rheum 31:37–43
12. Amis AA, Dowson D, Wright V, Miller JH (1979) The derivation of the elbow joint forces and their relation to prosthesis design. J Med Eng Technol 3:229–234
13. Amis AA, Dowson D, Wright V (1980) Elbow joint force predictions for some strenuous isometric actions. J Biomech 13:765–775
14. Halls AA, Travill R (1964) Transmission of pressure across the elbow joint. Anat Rec 150:243–247
15. Morrey BF, An KN, Stormont TJ (1988) Force transmission through the radial head. J Bone Jt Surg 70-A:250–256
16. McIlwain HH (2003) Glucocorticoid-induced osteoporosis: pathogenesis, diagnosis, and management. Prev Med 36:243–249
17. Solomon DH, Levin Elaine, Helfgott SM (2000) Patterns of medication use before and after bone densitometry: factors associated with appropriate treatment. J Rheumatol 27:1496–1500
18. Minaur NJ, Kounail D, Vedi S, Compston JE, Beresford JN, Bhalla K (2002) Methotrexate in the treatment of rheumatoid arthritis. II. In vivo effects on bone mineral density. Rheumatology 41:741–749
19. Dolan AL, Moniz C, Abraha H, Pitt P (2002) Does active treatment of rheumatoid arthritis limit disease-associated bone loss? Rheumatology 41:1041–1047

A three-dimensional quantitative analysis of carpal deformity in rheumatoid wrists

S. Arimitsu,
T. Murase,
J. Hashimoto,
K. Oka,
K. Sugamoto,
H. Yoshikawa,
H. Moritomo

From Osaka University Graduate School of Medicine, Osaka, Japan

We have measured the three-dimensional patterns of carpal deformity in 20 wrists in 20 rheumatoid patients in which the carpal bones were shifted ulnarwards on plain radiography. Three-dimensional bone models of the carpus and radius were created by computerised tomography with the wrist in the neutral position. The location of the centroids and rotational angle of each carpal bone relative to the radius were calculated and compared with those of ten normal wrists.

In the radiocarpal joint, the proximal row was flexed and the centroids of all carpal bones translocated in an ulnar, proximal and volar direction with loss of congruity. In the midcarpal joint, the distal row was extended and congruity generally well preserved. These findings may facilitate more positive use of radiocarpal fusion alone for the deformed rheumatoid wrist.

• S. Arimitsu, MD, Orthopaedic Surgeon
• T. Murase, MD, PhD, Assistant Professor
• J. Hashimoto, MD, PhD, Associate Professor
• K. Oka, MD, Orthopaedic Surgeon
• K. Sugamoto, MD, PhD, Professor
• H. Yoshikawa, MD, PhD, Professor
• H. Moritomo, MD, PhD, Assistant Professor
Department of Orthopaedic Surgery
Osaka University Graduate School of Medicine, 2-2, Yamada-oka, Suita, Osaka 565-0871, Japan.

Correspondence should be sent to Dr S. Arimitsu; e-mail: sayu@df6.so-net.ne.jp

doi:10.1302/0301-620X.89B4.18476 $2.00

J Bone Joint Surg [Br] 2007;89-B:490-4.
Received 31 July 2006; Accepted after revision 5 December 2006

The most common deformity of the wrist in rheumatoid arthritis (RA) has been described as carpal supination with ulnar translocation[1] and many reports have attempted to evaluate this deformity.[2-8] However, they have been two-dimensional studies based generally on radiological assessment, the value of which is limited because the complex, overlapping appearance makes measurement difficult, especially in wrists with severe deformity. We have therefore undertaken an analysis of such deformities using a new three-dimensional (3D) technique.

Patients and Methods

We studied 20 wrists in 20 rheumatoid patients in which there was ulnar translocation on the anteroposterior radiograph. We chose wrists with a carpal-ulnar distance ratio below 0.27[9] and in which the shape of each bone was easily recognisable (Fig. 1). There were 19 women and one man with a mean age of 61 years (21 to 80). The mean duration of the disease was 15 years (6 to 38). A total of 18 patients had the more erosive subset of the disease, one the less erosive[10] and one juvenile RA. For comparison, we also chose a control group of ten normal wrists in ten men with a mean age of 41.4 years (18 to 76).

Imaging. Computerised tomography (CT) with a slice thickness of 0.625 mm was undertaken on a clinical helical-type scanner (LightSpeed Ultra16; General Electric, Maukesha, Wisconsin). During image acquisition, the wrists were in the neutral position with the axes of the third metacarpal and forearm aligned. The data were saved in a standard format (DICOM; Digital Imaging and Communications in Medicine).

Segmentation and construction of three-dimensional surface bone models. Segmentation is the extraction of individual bony regions. The anatomy or region of interest must be delineated and separated so that it can be viewed individually and 3D models reconstructed. Regions of individual bones were segmented semi-automatically using a software program for image analysis (Virtual Place-M; AZE Ltd, Tokyo, Japan). Surface models of the radius and each carpal bone were obtained by 3D surface generation of the bone cortex.[11-13]

Measurement of centroid translocation and carpal rotation. First, the position of the volume centroid of any bone was calculated from the CT files.[14] In order to measure the translocation, we defined the grid for the lower radius and each carpal bone within it. This was the orthogonal reference system originally advocated by Belsole et al[15] (Figs 2 and 3). For the radius this was determined as follows: The Y axis was the longitudinal radial axis and indicated the proximal (+)/distal (-) direction; the Z axis was the line through the styloid perpendicular to the Y axis and indicated radial (+)/ulnar (-) displacement; the X axis was the

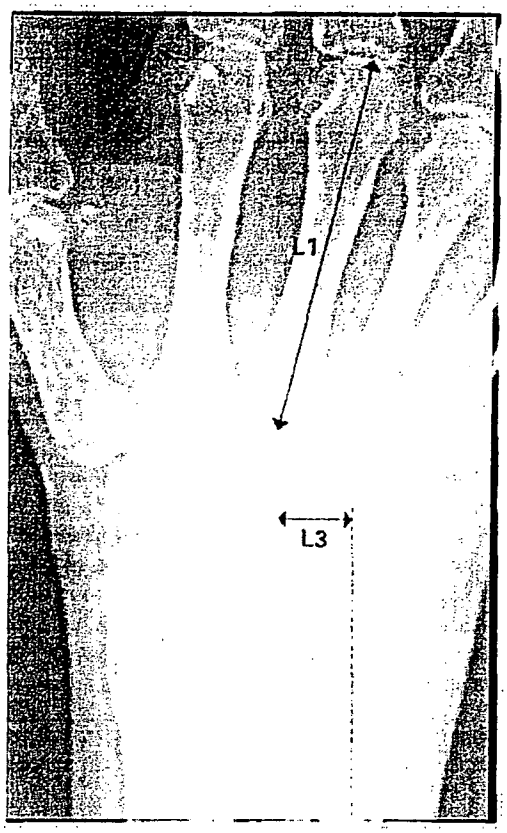

Fig. 1

Radiograph showing measurement of the carpal-ulnar distance ratio. It is calculated as L3/L1 where L3 is the distance between the centre of the capitate and the bony axis of the ulna and L1 the length of the third metacarpal. The normal ratio is 0.3 SD 0.03.

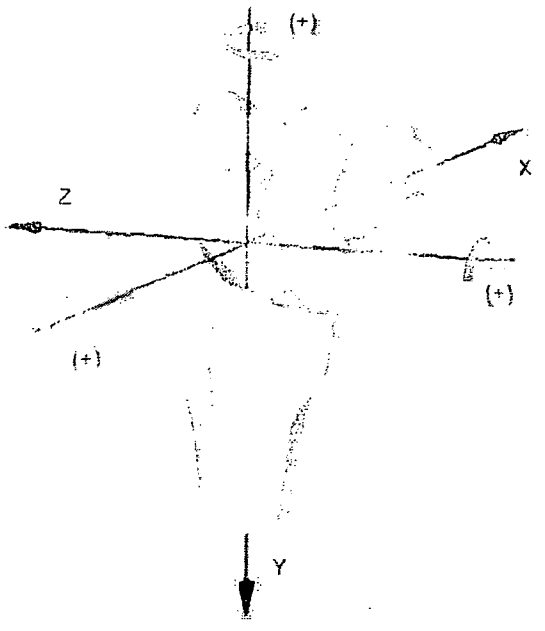

Fig. 2

A three-dimensional model showing details of the orthogonal reference system established in the radius as advocated by Belsole et al.[15] The Y axis was the longitudinal radial axis and indicated the proximal (+)/distal (-) direction; the Z axis was the line through the styloid perpendicular to the Y axis and indicated radial (+)/ulnar (-) displacement; the Y axis was the line perpendicular to the YZ plane and indicated palmar (+)/dorsal (-) displacement. Rotation around the Z axis produced flexion (+)/extension (-); that around the Y axis pronation (+)/supination (-) and that around the X axis indicated ulnar (+)/radial (-) deviation.

line perpendicular to the YZ plane and indicated palmar (+)/dorsal (-) displacement. Rotation around the Z axis produced flexion (+)/extension (-); that around the Y axis pronation (+)/supination (-) and that around the X axis indicated ulnar (+)/radial (-) deviation (Fig. 2). Thus, we calculated as a 3D vector the translocation of each carpal bone relative to the reference system determined for the radius.[13,15]

Next, using the anatomical feature as described by Belsole et al[14] the local co-ordinate system for the scaphoid, lunate, and capitate was established to characterise carpal direction (Fig. 3). The X axis of the scaphoid was defined as its principal axis, calculated as the line on which the moment of inertia was smallest and which ran through the centroid. The Z axis was defined as the line running through the dorsal ridge of the scaphoid in the plane perpendicular to the X axis and the Y axis was the line perpendicular to the XZ plane. The X axis of the lunate was defined as the line through the palmar and dorsal poles, the Y axis as the line through the centroid, perpendicular to the X axis and the Z axis as the line perpendicular to the XY plane. The Y axis of the capitate was defined as its principal axis[14] and the Z axis as the line through the dorsal joint ridge of the capitate-hamate joint perpendicular to the Y axis, rotated +90° around the Y axis. The X axis was the line perpendicular to the YZ plane. From these planes the 3D vector of a carpus relative to the radius was calculated with six degrees of freedom using the Euler angle[12] method. This quantified the direction and rotation of each carpal bone in the RA wrist relative to the radius and compared their positions with those of a normal wrist.

With regard to evaluating the translocation of location of the centroid, the variation in size of each carpal bone needed to be considered, and the translocation index was used for the purpose. It was calculated by dividing each of the three components of the vector of the centroids of the carpal bones by the square root of the cross-section of the radius at a plane perpendicular to its longitudinal axis and passing through Lister's tubercle[16] (Fig. 4).

The translocation index was as follows:

$$(Tx, Ty, Tz) = x/\sqrt{S}, y/\sqrt{S}, z\sqrt{S}),$$

where x, y and z represent the vectors of the centroid of the carpal bone, relative to the origin of the reference of the

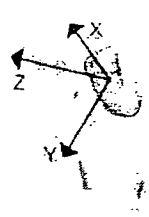

Fig. 3a

Fig. 3b

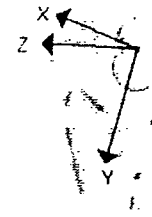

Fig. 3c

Diagram showing the orthogonal system as applied to a) the scaphoid, b) the lunate and c) the capitate according to Belsole et al.[14] The X axis of the scaphoid was defined as its principal axis, calculated as the line on which the moment of inertia was smallest and which ran through the centroid. The Z axis was defined as the line running through the dorsal ridge of the scaphoid in the plane perpendicular to the X axis, and the Y axis was the line perpendicular to the XZ plane. The X axis of the lunate was defined as the line through the palmar and dorsal poles, the Y axis as the line through the centroid, perpendicular to the X axis, and the Z axis as the line perpendicular to the XY plane. The Y axis of the capitate was defined as its principal axis and the Z axis as the line through the dorsal joint ridge of the capitate-hamate joint perpendicular to the Y axis, rotated +90° around the Y axis. The X axis was the line perpendicular to the YZ plane.

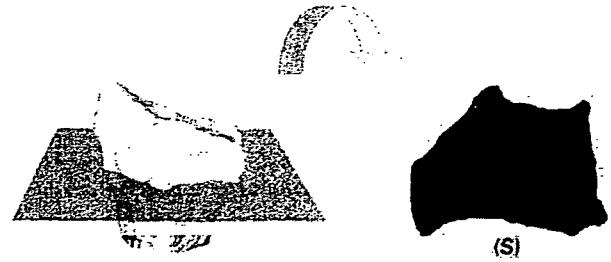

Fig. 4

Diagram showing the cross-section of the radius through Lister's tubercle, perpendicular to the longitudinal axis, S was the cross-sectional area of the radius (mm^2).

radius (mm) and S was the cross-sectional area of the radius (mm^2), at a plane perpendicular to its longitudinal axis at the level of Lister's tubercle (Fig. 4).

Statistical analysis. The left hand was converted to the orientation of the right and comparison of the results between the control and RA groups performed using standard statistical formulae based on the Mann-Whitney U-test. The results were deemed to be significant if $p \leq 0.05$.

Results

Centroid translocation. Three-dimensional images of the carpal bones showed that all centroids translocated not just in an ulnar direction, but also in the ulnar, proximal and volar direction, along the slope of the surface of the distal radius (Figs 5 and 6). Contacts between the radius and the scaphoid and the radius and the lunate were translocated ulnopalmarly and were incongruent in most cases. In the midcarpal joint, congruity was relatively well preserved compared with that of the radiocarpal joint in most cases (Fig. 7) while their radiographs showed joint narrowing (Fig. 1).

In the radioulnar deviation plane, the capitate ($p = 0.0011$) hamate, ($p = 0.0013$), lunate ($p < 0.0001$), scaphoid ($p = 0.0003$), triquetrum ($p < 0.0001$) and trapezoid ($p = 0.0197$), in RA wrists were significantly translocated to the ulnar side by a mean of 6.28, 4.68, 5.07, 7.10, 3.85 and 6.12 mm, respectively (Table I). In the flexion-extension plane all the centroids translocated in the palmar and proximal directions relative to the radius. The capitate ($p = 0.0083$), hamate ($p = 0.0037$) and scaphoid ($p = 0.0064$) in RA wrists were significantly translocated in the palmar direction by a mean of 3.21, 2.99 and 2.04 mm, respectively (Table I). The capitate ($p < 0.0001$), hamate ($p = 0.0037$), lunate ($p < 0.0001$), scaphoid ($p < 0.0001$) triquetrum ($p = 0.0011$), trapezium ($p < 0.0001$) and trapezoid ($p < 0.0001$) in RA wrists were significantly translocated proximally by a mean of 10.70, 9.41, 8.68, 6.90, 9.89, 11.37 and 13.30 mm, respectively (Table I).

Carpal rotation. The proximal row of RA wrists was flexed significantly compared with the normal wrists (Fig. 7b), the scaphoid at 25° ($p = 0.0003$) and the lunate at 10° ($p = 0.0311$) more than normal. In the pronation/supination plane, the scaphoid, lunate, and capitate did not supinate but were pronated 12°, 7° and 6°, respectively ($p = 0.053$, 0.147 and 0.356). The distal row was extended dorsally (Fig. 7c), as was the capitate by 12° ($p = 0.0387$) more than normal. The 3D images showed that the dorsally extended distal row corrected the hand to almost normal relative to the radius, by counteracting the flexion deformity of the proximal row.

Discussion

In the RA wrist, ligamentous laxity is probably the major cause of collapse and instability.[1] There are many reports which have attempted to measure the deformity radiologically,[2-4,6-8] but two-dimensional evaluation is of limited value. In our study, 3D imaging showed clearly that the rheumatoid carpus translocated obliquely in an ulnar, proximal and volar direction (Fig. 6). This quantitative technique allowed an easier understanding of this complex deformity. The direction of carpal translocation followed the natural slope of the joint surface of the distal radius which had a mean inclination of 24° in the coronal and 11° in the sagittal plane.[16,17] In normal wrists, displacement of the carpus was resisted mainly by the palmar and dorsal radiotriquetral and palmar radiolunate ligaments.[6,18,19] Their laxity probably allowed the 3D oblique translocation.

Rotational deformity, one of the most common deformities in RA, has been described qualitatively as carpal supination. Our 3D study, however, showed quantitatively that the main rotational deformity of the proximal row was

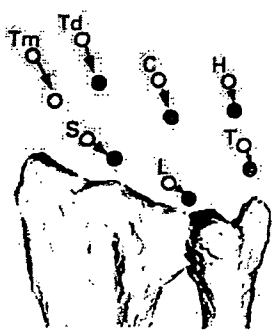

Fig. 5a

Fig. 5b

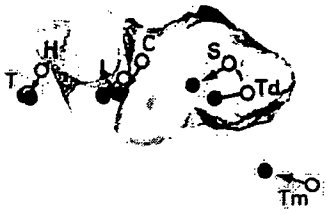

Fig. 5c

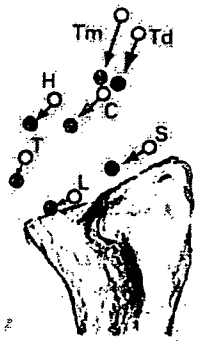

Fig. 5d

Diagrams showing centroid translocation from a) a dorsal view, b) ulnar view, c) distal view and d) radiopalmar view. All the centroids translocated in an ulnar, proximal and volar direction. The trapezium translated slightly in a dorsal direction according to the X component but, overall, translocated in a palmar direction (Tm, trapezium; Td, trapezoid; C, capitate; H, hamate; S, scaphoid; L, lunate; and T, triquetrum).

Fig. 6a

Fig. 6b

Three-dimensional radiopalmar view of the translation of the carpus in a) a normal wrist and b) rheumatoid arthritis. The carpus translocates along the direction of the slope of the joint surface of the distal radius.

Fig. 7a

Fig. 7b

Fig. 7c

A three-dimensional view showing carpal rotation and joint congruity. Figure 7a – The normal wrist. Figure 7b – The radiocarpal joint is incongruent (arrow). Figure 7c – Joint congruity is relatively well-preserved in the midcarpal joint (arrowheads). In the sagittal plane, the scaphoid and lunate are flexed as in b) and the capitate is extended as in c).

palmar flexion with no significant rotation. Accurate estimation of carpal supination by plain radiography may not be easy since palmar subluxation of the distal radius in relation to the ulna makes it difficult to obtain a true lateral view for measurement of carpal rotation in the transverse plane.

We also noticed a different pattern of rotational deformity between the radiocarpal and midcarpal joints. Our 3D study showed that the proximal row as flexed at the radiocarpal joint and the distal row extended at the midcarpal joint (Fig. 7). While flexion of the proximal row was associated with translocation, the extension of the distal row was associated only with minor translocation. Although our patients had joint narrowing throughout the carpus, the congruity and function of the midcarpal joint were better preserved even in deformed RA wrists than at the radiocarpal joint.

Moritomo et al[20] proposed a self-stabilising mechanism which is stronger in the midcarpal than in the radiocarpal joint. A scaphoid under axial load against the trapezium tends to rotate in a flexion/ulnar direction. This turning effect is constrained by the extension/radial deviation moment of the triquetrum, leading to a stable equilibrium provided that the interosseous ligaments in the proximal row are intact. We speculated that, with loosening of many carpal ligaments, the radiocarpal joint may easily lose congruity. Whereas the deformity in this joint included translational and rotational elements, in the midcarpal joint the deformity was predominantly rotational. We considered the radiocarpal joint to be more incongruent and thereby more prone to cartilaginous damage.

Our study has limitations, the most important of which is that it was based on selected cases in which the whole carpal bones were shifted to the ulnar side, but the shapes were relatively recognisable on plain radiography. The other limitation was that age and gender were not fully matched between the RA and control wrists. It is possible that calculation of centroids and angles of rotation are influenced by erosion of the carpal bones with a subsequent alteration of shape. Our quantitative information,

Table I. Details of translocation in the carpal bones

	Centroid translocation																							
	Capitate				Hamate				Lunate				Scaphoid				Triquetrum				Trapezium				Trapezoid			
Direction	AD* (mm)	TI†		SD	AD (mm)	TI		SD	AD (mm)	TI		SD	AD (mm)	TI		SD	AD (mm)	TI		SD	AD (mm)	TI		SD	AD (mm)	TI		SD
Palmar																								
Normal	3.21	0.01		0.11	2.99	0.07		0.11	1.08	0.23		0.05	2.04	0.23		0.07	0.52	0.15		0.08	0.22	0.47		0.18	0.33	0.04		0.16
RA‡		0.17		0.16		0.22		0.21		0.33		0.18		0.37		0.16		0.20		0.21		0.54		0.16		0.07		0.17
Proximal																								
Normal	10.70	-0.57		0.14	9.41	-0.61		0.24	8.68	0.05		0.14	6.90	-0.20		0.06	9.89	-0.19		0.24	11.37	-0.83		0.16	13.30	-0.82		0.16
RA		-0.15		0.20		-0.26		0.20		0.48		0.27		0.10		0.15		0.25		0.27		-0.42		0.16		-0.32		0.17
Ulnar																								
Normal	6.28	0.19		0.19	4.68	0.70		0.19	5.07	0.35		0.09	7.10	-0.24		0.14	3.85	0.84		0.10	6.42	-0.49		0.26	6.12	-0.24		0.25
RA		0.52		0.18		1.04		0.23		0.66		0.14		0.05		0.14		1.17		0.16		-0.27		0.18		0.00		0.17

* AD, the absolute value of the difference of the mean translation (mm)
† TI, translocation index
‡ RA, rheumatoid arthritis

however, allowed early identification of the rheumatoid deformity and should be a guide to treatment, in particular in the decision as to whether to undertake radiocarpal fusion alone or to include the midcarpal joint.

Supplementary Material

A further opinion by Dr Klemens Trieb is available with the electronic version of this article on our website at www.jbjs.org.uk

No benefits in any form have been received or will be received from a commercial party related directly or indirectly to the subject of this article.

References

1. **Shapiro JS.** The wrist in rheumatoid arthritis. *Hand Clin* 1996;12:477-98.
2. **Kushner DM, Braunstein EM, Buckwalter KA, Krohn K, White HA.** Carpal instability in rheumatoid arthritis. *Can Assoc Radiol J* 1993;44:291-5.
3. **Murametsu K, Ihara K, Tanaka H, Kawai S.** Carpal instability in rheumatoid wrists. *Rheumatol Int* 2004;24:34-6.
4. **Shapiro JS.** A new factor in the etiology of the ulnar drift. *Clin Orthop* 1970;68:32-43.
5. **Taleisnik J.** Rheumatoid synovitis of the volar compartment of wrist joint: its radiological signs and its contribution to wrist and hand deformity. *J Hand Surg [Am]* 1979;4:526-35.
6. **Flury MP, Herren DB, Simmen BR.** Rheumatoid arthritis of the wrist: classification related to the natural course. *Clin Orthop* 1999;366:72-7.
7. **Van Vught RM, van Jaarsveld CH, Hofman DM, Helders PJ, Bijlsma JW.** Patterns of disease progression in the rheumatoid wrist: a long-term follow-up. *J Rheumatol* 1999;26:1467-73.
8. **Shapiro JS.** Wrist involvement in rheumatoid arthritis swan-neck deformity. *J Hand Surg [Am]* 1982;7:484-91.
9. **Youm Y, McMurtry RY, Platt AE.** Kinematics of the wrist: an experimental study of radial-ulnar deviation and flexion-extension. *J Bone Joint Surg [Am]* 1978;60-A:423-31.
10. **Ochi T, Iwase R, Kimura T, et al.** Effect of early synovectomy on the course of rheumatoid arthritis. *J Rheumatol* 1991;18:1794-8.
11. **Lorensen WE, Cline HE.** Marching cubes: a high resolution 3D surface construction algorithm. *Computer Graphics* 1987;21:163-9.
12. **Goto A, Moritomo H, Murase T, et al.** In vivo three-dimensional wrist motion analysis using magnetic resonance imaging and volume-based registration. *J Orthop Res* 2005;23:750-6.
13. **Oka K, Moritomo H, Murase T, et al.** Patterns of carpal deformity in scaphoid nonunion: a 3-dimensional and quantitative analysis. *J Hand Surg [Am]* 2005;30:1136-44.
14. **Belsole RJ, Hilbelink DR, Llewellyn JA, et al.** Mathematical analysis of computed carpal models. *J Orthop Res* 1988;6:116-22.
15. **Belsole RJ, Bilbelink DR, Llewellyn JA, Dale M, Ogden JA.** Carpal orientation from computed reference axes. *J Hand Surg [Am]* 1991;16:82-90.
16. **Palmer AK.** Fractures of the distal radius. In: Green DP, ed. *Operative hand surgery.* Vol. 1. Third ed. New York: Churchill Livingstone, 1993:929-73.
17. **Schuind FA, Linscheid RL, An KN, Chao EY.** A normal data base of posteroanterior roentgenographic measurements of the wrist. *J Bone Joint Surg [Am]* 1992;74-A:1418-29.
18. **Cooney WP, Garcia-Elias M, Dobyns JH.** Anatomy of mechanics of carpal instability. *Surg Rounds Orthop* 1989;3:15-24.
19. **Mizuseki T, Ikuta Y.** The dorsal carpal ligament: their anatomy and function. *J Hand Surg [Br]* 1989;14:91-8.
20. **Moritomo H, Murase T, Goto A, et al.** In vivo three-dimensional kinematics of the midcarpal joint of the wrist. *J Bone Joint Surg [Am]* 2006;88-A:611-21.

DNA RESEARCH 13, 169–183 (2006) doi:10.1093/dnares/dsl006

Isolation and Expression Profiling of Genes Upregulated in Bone Marrow-Derived Mononuclear Cells of Rheumatoid Arthritis Patients

Nobuo NAKAMURA,[1,†] Yasunori SHIMAOKA,[2,†] Takahiro TOUGAN,[3] Hiroaki ONDA,[3,4] Daisuke OKUZAKI,[3] Hanjun ZHAO,[3] Azumi FUJIMORI,[3] Norikazu YABUTA,[3] Ippei NAGAMORI,[3] Akie TANIGAWA,[4] Jun SATO,[3] Takenori ODA,[5] Kenji HAYASHIDA,[6] Ryuji SUZUKI,[7] Masao YUKIOKA,[2] Hiroshi NOJIMA,[3,4,*] and Takahiro OCHI[7]

Center of Arthroplasty, Kyowakai Hospital, Suita, Japan[1], Yukioka Hospital, Osaka, Japan[2], Department of Molecular Genetics, Research Institute for Microbial Diseases, Osaka University, 3-1 Yamadaoka, Suita, Osaka 562-0031, Japan[3], Innovation Plaza Osaka, Izumi, Japan[4], Department of Rheumatology, NHO Osaka-Minami Medical Center, Kawachinagano, Japan[5], Hoshigaoka Kosei-Nenkin Hospital, Hirakata, Japan[6] and Clinical Research Center for Allergy and Rheumatology, National Sagamihara Hospital, 18-1 Sakura-dai, Sagamihara, Kanagawa 228-8522, Japan[7]

(Received 25 July 2006; revised 21 August 2006)

Abstract

We have comprehensively identified the genes whose expressions are augmented in bone marrow-derived mononuclear cells (BMMC) from patients with Rheumatoid Arthritis (RA) as compared with BMMCs from Osteoarthritis (OA) patients, and named them *AURA* after *au*gmented in *RA*. Both stepwise subtractive hybridization and microarray analyses were used to identify *AURA* genes, which were confirmed by northern blot analysis and/or reverse transcription polymerase chain reaction (RT–PCR). We also assessed their expression levels in individual patients by quantitative real-time RT–PCR. Of 103 *AURA* genes we have identified, the mRNA levels of the following 10 genes, which are somehow related to immune responses, were increased in many of the RA patients: *AREG* (=*AURA*9), FK506-binding protein 5 (FKBP5 = *AURA4*5), C-type lectin superfamily member 9 (*CLECSF9* = *AURA2*4), tyrosylprotein sulfotransferase 1 (*TPST1* = *AURA5*2), lymphocyte G0/G1 switch gene (*G0S2* = *AURA*8), chemokine receptor 4 (CXCR4 = *AURA8*6), nuclear factor-kappa B (NF-κB = *AURA2*5) and two genes of unknown function (FLJ11106 = *AURA1*, BC022398 = *AURA*2 and XM_058513 = *AURA1*7). Since *AREG* was most significantly increased in many of the RA patients, we subjected it to further analysis and found that AREG-epidermal growth factor receptor signaling is highly activated in synovial cells isolated from RA patients, but not in OA synoviocytes. We propose that the expression profiling of these *AURA* genes may improve our understanding of the pathogenesis of RA.

Key words: stepwise subtraction; microarray; RA; OA; amphiregulin; synoviolin

1. Introduction

Rheumatoid arthritis (RA) is a systemic autoimmune disease characterized by arthritis that predominantly results in chronic inflammation of systemic joints associated with the overgrowth of synovial cells. This induces progressive cartilage and bone destruction in the joint and subsequent disability. Since RA pathogenesis is likely to involve genetic elements, a number of groups have subjected samples from healthy and affected individuals to DNA microarray analyses for a broad-scale comparison. These studies have provided

Communicated by Mitsuo Oshimura

* To whom correspondence should be addressed. Tel. +81-6-6875-3980, Fax. +81-6-6875-5192, E-mail: snj-0212@biken.osaka-u.ac.jp

† These authors contributed equally to this work.

significant insights into RA pathogenesis.[1,2] The first samples tested were synovial specimens,[3–8] and peripheral blood mononuclear cells (PBMC),[9] from RA and osteoarthritis (OA) patients, and cluster analysis of the resulting microarray gene-expression data revealed some candidate genes that may play a specific role in RA pathogenesis.

In other studies searching for key factors in RA pathogenesis, immunoscreening by using an antirheumatoid synovial cell antibody identified synoviolin/Hrd1 to be a highly expressed enzyme (E3 ubiquitin ligase) in the rheumatoid synovium.[10] Synoviolin appears to be a pathogenic factor for RA because mice overexpressing this enzyme developed spontaneous arthropathy, while heterozygous knockdown results in increased synovial cell apoptosis and resistance to collagen-induced arthritis.[11] It was proposed that the excess elimination of unfolded proteins due to synoviolin overexpression triggers synovial cell overgrowth.[12] Thus, synoviolin may play a pivotal role in the pathogenesis of arthropathy due to its functions in the quality control of proteins through the endoplasmic reticulum (ER)-associated degradation (ERAD) system; its elevated expression may therefore have an anti-apoptotic effect that causes synovial hyperplasia.

Bone marrow-derived mononuclear cells (BMMC) are another target for analyses aiming to identify the key genes that participate in RA pathogenesis because accumulating evidence suggests that BMMC cell abnormalities may contribute to the pathogenesis of RA and experimental arthritis models.[13–17] Moreover, RA patients suffer from defective central and peripheral B-cell tolerance checkpoints,[18] the first of which occurs in the bone marrow between the early immature and immature B-cell stages (the second counter selection step of autoantibody-expressing B cells takes place in the periphery, when the new emigrant becomes a mature naive B cell).[18,19] In addition, inflammatory changes similar to those found in RA synovium seem to occur in the subchondral bone marrow of the involved RA joint,[20] and synovial inflammatory tissue can reach the adjacent bone marrow by fully breaking the cortical barrier.[21] Thus, BMMC cells are an interesting subject for studies seeking to identify specific genes involved in RA pathogenesis.

To identify the genes whose expressions are dramatically induced or reduced in the pooled BMMC mRNAs of 50 RA patients as compared with 50 OA patients, we here subjected these pooled mRNAs to stepwise subtraction, which is a unique technique that we have developed previously.[22] This method permitted the comprehensive identification of those genes that are specifically up- or down-regulated during RA pathogenesis. In addition, we also used microarray analysis, since DNA microarray analyses on the BMMC of RA patients have not been described previously. As a control, we also subjected the BMMC RNA from OA patients to stepwise subtraction and microarray analysis to identify the genes that are specifically involved in OA pathogenesis. These analyses together resulted in the isolation of 103 RA-upregulated genes, of which amphiregulin (AREG) was revealed by quantitative real-time RT–PCR (QRT–PCR) to be the most conspicuously induced gene in RA patients. Interestingly, we also show here that AREG operates upstream of synoviolin in isolated synovial cells through an epidermal growth factor receptor (EFGR) signaling pathway. We discuss how AREG upregulation could contribute to RA pathogenesis.

2. Patients, Materials and Methods

2.1. Human subjects and ethical considerations

All RA patients satisfied the 1987 revised diagnostic criteria of the American College of Rheumatology (ACR: formerly the American Rheumatism Association).[23] All OA patients fulfilled the ACR criteria for hip or knee OA.[24] The RA and OA patient groups were largely matched in terms of their average age and sex (Supplementary Figure S1A and B). This study was reviewed and approved by the Internal Review Board of the Research Institute for Microbial Diseases, Osaka University. Accordingly, a written informed consent was obtained from each participant before obtaining human tissues.

2.2. Cell proliferation assay

The synovial cells from each patient were seeded onto uncoated 35 mm tissue culture plates at 1×10^5 cells/well and cultured in 5% FBS/DMEM. After 12 h, the cells were incubated in fresh 5% FBS/DMEM with (100 ng/ml) or without AREG (Sigma-Aldrich, A 7080). Four photos were taken from fixed areas in four quadrants near the central area of each plate at the 0, 1, 3 and 4 day time points. The cells at each time point were counted from these four photos and expressed as mean ± standard error (SE).

2.3. Statistical analysis

Significant differences were determined using the Spearman's rank correlation (Supplemenatry Figure S4) or the Mann–Whitney *U*-test (Figs 2, 4 and Supplementary Figure S3). The data are expressed as means ± SE. $P < 0.05$ or $P < 0.01$ was considered to be statistically significant.

3. RESULTS

3.1. Identification of RA- or OA-specific genes by stepwise subtraction and DNA microarray analysis

To isolate the putative RA-specific genes that are upregulated in BMMC of RA patients relative to those

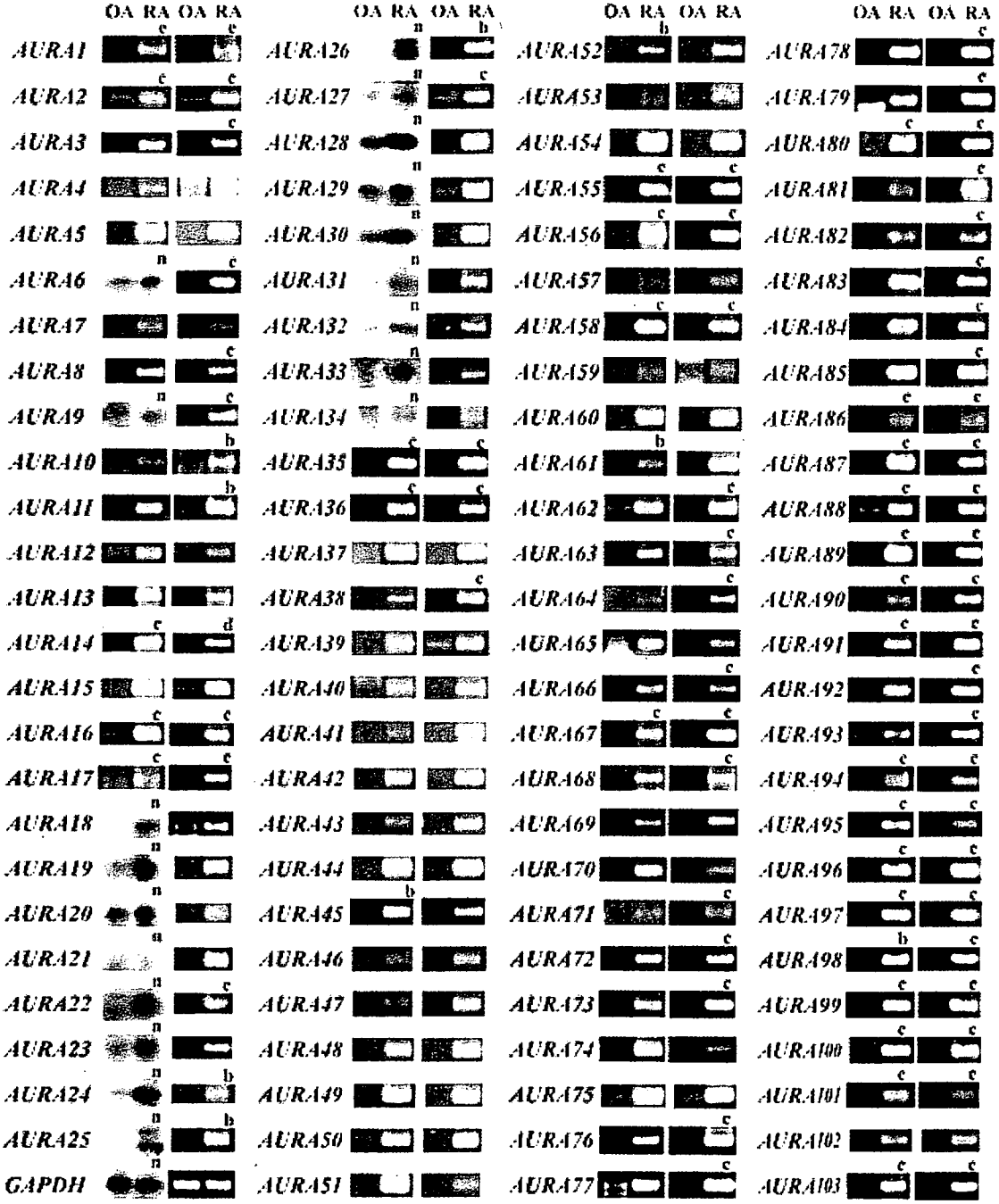

Figure 1. Northern blot or RT–PCR analysis of individual *AURA* cDNA clones to compare the expression levels of the genes in the BMMC of 50 RA patients and 50 OA patients (see Table 1 for their gene names). A northern blot or RT–PCR for *GAPDH* is also shown as a loading control. Left row: expression levels as detected by RT–PCR or northern blot analysis (denoted as n above each picture). Right row: confirmation of the expression level of each gene as determined by RT–PCR. The annealing temperature and amplification cycles for RT–PCR were always 50°C and 40 cycles, respectively, with the exception of the reactions denoted by a (50°C and 35 cycles, respectively), b (50°C and 30 cycles, respectively), c (55°C and 35 cycles, respectively), d (55°C and 40 cycles, respectively), and e (60°C and 40 cycles, respectively).

that are upregulated in OA patients, we first used our stepwise subtractive hybridization method. Briefly, we prepared a cDNA library from the pooled mRNA from the BMMC of 50 RA patients (Supplementary Figure S1A) by the linker-primer method using a pAP3neo vector.[25] Stepwise subtractive hybridization was then performed with the biotinylated pooled mRNA from the BMMC of 50 OA patients (Supplementary Figure S1A) to select candidate genes that may show upregulation in RA BMMC only as described previously.[22] To examine if the candidate genes are actually upregulated in RA but not OA BMMC, we performed northern blot analysis and/or RT–PCR using the pooled mRNA from the BMMC of 50 RA and 50 OA patients (Fig. 1). To reduce

the possibility of missing important RA-specific pathogenic genes by this method, we also performed a genome-wide complementary DNA microarray analysis using the Agilent Hu44K array with the same pooled RNA samples obtained from the BMMC of RA and OA patients that were described above. When we tested top 70 genes from the microarray list of RA-upregulated genes by northern blot analysis and/or RT–PCR as described above, we found that only 20 genes really displayed RA-upregulated expressions. Thus, we identified 103 RA-upregulated genes (Fig. 1) and named them *AURA* (***au***gmented in ***RA***). As shown in Table 1, 15 *AURA* genes (*AURA1*~*AURA7* and *AURA10*~*AURA17*) are uncharacterized novel genes.

We also performed similar experiments to obtain candidate OA-upregulated genes by generating a cDNA library from the pooled mRNA from the BMMC of 50 OA patients (Supplementary Figure S1A) and then using biotinylated pooled mRNA from the BMMC of 50 RA patients for subtraction (Supplementary Figure S1A). DNA microarray analysis also yielded a number of candidate OA-specific genes, as described above. However, when we checked whether these candidate genes are truly specifically up-regulated in OA BMMCs by northern blot analysis and/or RT–PCR, we could confirm this for only two genes (Supplementary Figure S2). These two OA-upregulated genes encode nuclear receptor coactivator 1 and a hypothetical protein (FLJ20581). This result suggests that the gain of function due to the enhanced expression of the RA-upregulated candidate genes is important in the pathogenesis of RA. Thus, we subsequently concentrated our study on the RA-upregulated genes.

3.2. *Expression profiles of RA-upregulated genes in individual RA or OA patients*

To determine whether the upregulation of the 103 RA-specific candidate genes is widespread in many RA patients or occurs in only a few patients, we performed QRT–PCR using individually prepared RNA samples from the BMMC or PBMC of RA patients. Of the 103 candidate genes, 5 genes whose functions are unknown and 12 genes that may be related to growth regulation or immune response were analyzed by QRT–PCR. OA patients were also examined as negative controls. In every QRT–PCR, a standard RNA from the PBMC of a healthy volunteer (male, age 52) was used (denoted as normal with a relative intensity of 1.0). This allowed us to compare the expression profiles of the genes tested in this study. In addition, since we used this control, we could also compare the expression profiles of the genes in this study with those of other genes tested in our previous reports on other autoimmune diseases.[26]

Of the 17 tested *AURA* genes (denoted x in Table 1), AREG (*AURA9*) was the most conspicuously upregulated in the BMMC of many of the RA patients, while in contrast OA BMMCs invariably expressed this gene at very low levels (Fig. 2A). Similarly, the PBMC of many RA patients strongly expressed AREG, while only very low expression was detected in the PBMC of the OA patients (Fig. 2A). AREG is one of the EGF-like growth factors that stimulate cell growth by activating the EGF receptor (EGFR) signaling of the target cells in an autocrine/juxtacrine fashion.[27]

AURA1 was the next most conspicuously upregulated gene in the BMMC of many RA patients, while the BMMC of all OA patients showed only very low expression of this gene (Fig. 2B). However, unlike *AREG*, the PBMC of RA patients showed negligible enhancement in the expression of *AURA1*. *AURA1* encodes an uncharacterized protein containing a thioesterase domain (Fig. 2B inset) that may cleave thioester bonds of an unknown target.

The gene encoding FK506 (tacrolimus)-binding protein 5 (FKBP5 = *AURA45*) also showed enhanced expression in nearly half of the RA patient BMMC samples, while no such increase was observed in the OA patient BMMC samples or in the PBMC of the RA patients (Fig. 2C). FKBP5 is a cellular receptor for FK506 and has an immunosuppressive effect on activated T cells because it inhibits the protein phosphatase calcineurin.[28]

Nearly half of the RA patient BMMC samples showed 5- to 50-fold greater expression of *CLECSF9* (=*AURA24*), *TPST1* (=*AURA52*) and *AURA2* than the normal control PBMC sample (Fig. 2D–F). No such increase was observed in the BMMC of OA patients or in the PBMC of the RA patients. *CLECSF9* encodes a macrophage-inducible C-type lectin (Mincle) that harbors a calcium-dependent carbohydrate-recognition domain. *TPST1* is one of the two Golgi tyrosylprotein sulfotransferases (*TPST1* and *TPST2*) that mediate the post-translational modification tyrosine O-sulfation.

G0S2 (=*AURA8*), chemokine receptor 4 (CXCR4 = *AURA86*), nuclear factor-kappa B (NF-κB = *AURA25*) and *AURA17* showed augmented expression in both the BMMC and PBMC of some of the RA patients when compared to the expression in the BMMC and PBMC of the OA patients, although the differences between the RA and OA samples are not as significant as for the previously discussed genes (Supplementary Figure S3A–D). G0S2 is one of the G0/G1 switch (G0S) genes that are differentially expressed in lymphocytes during their lectin-induced switch from the G0 to the G1 phases of the cell cycle.[29] CXCR4, the receptor for a chemokine called stromal cell-derived factor-1 (SDF-1/CXCL12), is important in the migration, homing and survival of hematopoietic stem cells. SDF-1, which is secreted by ischemic myocardium, is involved in the homeostatic and inflammatory traffic of leukocytes, and is highly expressed in the synovial tissues of RA patients.[30] NF-κB

Table 1. List of *AURA* genes

AURA no.	Accession no.	Sequence description	SS/DM	QRT–PCR
AURA1	AK001968	Unknown cDNA (FLJ11106)	b	r
AURA2	BC022398	Unknown cDNA	b	r
AURA3	BC031341	Unknown cDNA (hypothetical protein MGC45871)		
AURA4	NM_052862.2	Unknown cDNA (hypothetical protein MGC21854)		
AURA5	AK097275.1	Unknown cDNA (FLJ39956) L-PLASTIN-like		
AURA6	BC019355	Unknown cDNA (ring finger protein 149: IMAGE:3956746)		
AURA7	AF078845.1	Unknown cDNA (16.7Kd protein)		
AURA8	M69199	Putative lymphocyte G0/G1 switch gene (G0S2)=Aile1	b	r
AURA9	AH002608	Amphiregulin	b	r
AURA10	AK026118	Unknown cDNA (Ch20-ORF43)		r
AURA11	AK094006	Unknown cDNA		
AURA12	AK095896.1	Unknown cDNA (FLJ38577)		
AURA13	BC014435	Unknown cDNA (IMAGE:4855747)		r
AURA14	ZF161365	Unknown cDNA (HSPC102)	m	
AURA15	FLJ23431	Unknown cDNA (FLJ23431) MHC class I -like		
AURA16	BC066334	Unknown cDNA (FLJ37760)		
AURA17	XM_058513	Unknown cDNA (DKFZp434H2111)	m	r
AURA18	BC016660	Heat shock 70 kDa protein 8		
AURA19	BC022347	Lactotransferrin		
AURA20	NM_001800.2	Cyclin-dependent kinase inhibitor 2D (p19) (CDKN2D)		
AURA21	X55668.1	Proteinase 3		
AURA22	BC013946	Kruppel-like factor 13		
AURA23	BC022463	Dual specificity phosphatase 1 (DUSP1)		r
AURA24	AY358499	C-type lectin, superfamily member 9 (CLECSF9)	b	r
AURA25	AY033600	NF-kB alpha	b	r
AURA26	AF194172	Androgen-regulated protein 6 (AIG6)	m	
AURA27	NM_021810	Cadherin-like 26 (CDH26)		
AURA28	X52053.1	HP-1 (corticostatin/defensin family)		r
AURA29	BC018857.2	Translation elongation factor 1 gamma		
AURA30	BC053585.1	Colony stimulating factor 3 receptor (granulocyte)		
AURA31	AY124010	Interleukin 1 receptor, type II (IL1R2)	m	
AURA32	BC020635	Ficolin 1 (FCN1: collagen/fibrinogen domain-containing)		
AURA33	BC106068	Microtubule-associated protein, RP/EB family, member 1		
AURA34	AF443591	Death effector domain-containing DNA binding protein2		
AURA35	BC032491	Ubiquitin-conjugating enzyme E2L 6 (UBE2L6)		
AURA36	BC004967	Ubiquitin associated domain containing 1 (UBADC1)		
AURA37	NM_006313.1	Ubiquitin specific protease 15 (USP15)		
AURA38	BC011358	ADP-ribosylation factor 1		
AURA39	AY366510.1	Pre-mRNA 3'end processing factor FIP1		
AURA40	NM_175039.1	Sialyltransferase 7D (SIAT7D). transcript variant 2		
AURA41	BC030230.2	Aminolevulinate, delta- synthase 2		
AURA42	NM_014390.1	Staphylococcal nuclease domain containing 1 (SND1)		
AURA43	NM_015999.2	Adiponectin receptor 1 (ADIPOR1)		
AURA44	BC033877.1	Finkel-Biskis-Reilly murine sarcoma virus (FBR-MuSV)		r
AURA45	NM_004117	FK506 binding protein 5 (FKBP5)	b	r
AURA46	NM_000211.1	Integrin beta 2 (antigen CD18 (p95)		
AURA47	BC015641.2	Enolase 1 (alpha)		

Table 1. continued.

AURA no.	Accession no.	Sequence description	SS/DM	QRT-PCR
AURA48	BC028299.1	Non-POU domain containing. octamer-binding.		
AURA49	BC000734.2	Eukaryotic translation initiation factor 3. subunit 648 kDa		
AURA50	NM_012198.2	Grancalcin. EF-hand calcium binding protein (GCA)		
AURA51	BC026690.2	CD97 antigen. transcript variant 2.		
AURA52	CR542060	Tyrosylprotein sulfotransferase 1 (TPST1)	m	r
AURA53	NM_005875.1	Translation factor sui1 homolog (GC20)		
AURA54	NM_004048.2	Beta-2-microglobulin (B2M)		
AURA55	BC017934	NudC domain containing 2 (NUDCD2)		
AURA56	NM_000569	Fc fragment of IgG, low affinity IIIa, receptor for (CD16)	b	
AURA57	BC018649.2	Polymerase (RNA) II (DNA directed)		
AURA58	BC013293	Synuclein, alpha (a molecular chaperone)		
AURA59	NM_033405.2	PRIC285		
AURA60	J02694.1	Myeloperoxidase		
AURA61	BC020219	Zinc finger protein 143 (clone pHZ-1)	m	
AURA62	BC071590	Nijmegen breakage syndrome 1 (nibrin)		
AURA63	BC003186	DNA replication complex GINS protein PSF2		r
AURA64	NM_006060	Zinc finger protein, subfamily 1A, 1 (ZNFN1A1)		
AURA65	BC015859	T-cell activation GTPase activating protein		
AURA66	Z50749	Sds22 (protein phosphatase regulatory subunit)-like		r
AURA67	AF411850	C-type lectin-like receptor CLEC-6	m	
AURA68	BC064831	HMT1 hnRNP methyltransferase-like 3		
AURA69	BC022797	Mof4 family associated protein 1		
AURA70	BC032437	Heterogeneous nuclear ribonucleoprotein A3		
AURA71	M87790	Anti-hepatitis A immunoglobulin lambda chain variable region		
AURA72	K01763	Haptoglobin alpha(1S)-beta precursor		
AURA73	BC016800	Aldolase A, fructose-bisphosphate, transcript variant		
AURA74	BC001391	Actin-like 6A, transcript variant 1		
AURA75	NM_003512.3	H2 histone, family 2AC (H2AC)		
AURA76	BC017558	H3 histone, family 3B (H3.3B)		
AURA77	BC032748	Myosin regulatory light chain MRCL3		
AURA78	S60099	APPH = amyloid precursor protein homolog		
AURA79	BC067100	Fas (TNFRSF6) associated factor 1		
AURA80	NM_000896	Cytochrome P450, family 4, subfamily F (CYP4F3)	b	
AURA81	BC010577	Granulin (an association partner of cyclin T1)		
AURA82	AF054186	p18		
AURA83	BC028626	Trinucleotide repeat containing 6B		
AURA84	L43631	Scaffold attachment factor B (SAF-B)		
AURA85	M11124	MHC HLA DQ alpha-chain mRNA from DRw9 cell line		
AURA86	AF025375	Chemokine (C-X-C motif) receptor 4 (CXCR4)	b	r
AURA87	BC000163	Vimentin (VIM)		
AURA88	BC071860	Lactate dehydrogenase B (LDHB)		
AURA89	BC100032	Ribosomal protein S13 (RPS13)		
AURA90	BC011852	Glutamine synthetase (GLUL)		
AURA91	NM_000045	Arginase, liver (ARG1)		
AURA92	BC006510	Cyclin B1		
AURA93	BC007063	Peroxiredoxin 1		
AURA94	NM_005746	Pre-B-cell colony enhancing factor 1 (PBEF1)	m	

Table 1. continued.

AURA no.	Accession no.	Sequence description	SS/DM	QRT–PCR
AURA95	BC018711	RNA-binding region (RNP1. RRM) containing 1		
AURA96	NM_001126	Adenylosuccinate synthase (ADSS)		
AURA97	BC008929	rab2 mRNA. YPT1-related and member of ras family		
AURA98	NM_004226	Serine/threonine kinase 17b (apoptosis-inducing) (STK17B)	m	
AURA99	BC096336	Insulin-degrading enzyme		
AURA100	AF501883	G protein Beta polypeptide 2 (GNB2)		
AURA101	BC007237	Myeloid/lymphoid or mixed-lineage leukemia		
AURA102	BC034149.1	Ribosomal protein S3		
AURA103	NM_020980	Aquaporin 9 (AQP9)	m	

Of 103 *AURA* genes, 83, 10 or 10 genes were identified by stepwise subtraction (SS) alone (no mark), by DNA microarray (DM) alone (denoted by m) or by both techniques (denoted by b), respectively. The *AURA* genes that were subjected to QRT–PCR analysis are denoted by r.
PRIC285: peroxisomal proliferator-activated receptor A interacting complex 285.

is a transcription factor that resides in the cytoplasm of every cell and translocates to the nucleus when activated by a wide variety of agents, including cytokines.[31] *AURA17* is an uncharacterized novel gene that encodes a large protein with 8 leucine rich repeats, Mitochondrial Rho (Miro) motif and protein tyrosine kinase domain (Supplementary Figure S3D inset).

We also tested seven other genes in RA and OA BMMC and PBMC samples by QRT–PCR, but none showed a widespread and conspicuous increase in expression in the RA BMMC samples (data not shown). Consequently, these genes appear to play a less significant role in RA pathogenesis. Since these experiments and those described above consumed almost all BMMC and PBMC samples from the RA and OA patients, the remaining *AURA* genes will have to be tested in the future with another RA patient set.

3.3. *Expression pattern of AURA genes in PBMC*

To determine whether the *AURA* genes are expressed in particular human blood cells, we performed RT–PCR on multiple tissue cDNA panels (MTC) from Clontech (Palo Alto, CA). As shown in Fig. 3, RT–PCR detected *AREG* mRNA in both monocytes (lane 4) and T and B cells (lanes 2–4), in particular in activated $CD4^+$ T cells (lane 8). *AURA1* is detected predominantly in resting $CD4^+$ (T helper/inducer; lane 3) and activated $CD4^+$ T (lane 8) cells. *CLECSF9* is expressed in most cell types except for activated $CD19^+$ T cells (lane 6), while *G0S2* is found primarily in monocytes (lanes a and 4). *FKBP5*, *TPST1*, *CXCR4*, *AURA2* and *NFκB* are ubiquitously expressed in most cell types. Thus, the analysis of the functions these *AURA* genes, apart from *AURA1* and *G0S2*, play in specific blood cells will not be easy because they are already expressed in normal blood. However, the function of *AURA1* can be studied by using $CD4^+$ T cells of RA and OA patients. In this study, however, we could not perform this analysis because of the low amounts of BMMC that we could obtain from the RA patients.

3.4. *AREG stimulates the growth of synovial cells*

Since AREG appears to be the most conspicuously unpregulated gene in many RA patients, we subjected it to further analysis. We first examined its ability to stimulate the growth of isolated synovial cells because AREG is one of the ligands of EGFR and is known to induce cell growth. Thus, we isolated synovial cells from synovial tissues that were obtained from five RA and three OA patients during joint reconstructive surgery. In the absence of AREG in the culture medium, the synovial cells from both the RA and OA patients grew at a similar rate (Fig. 4A and B). However, when AREG was present, the synovial cells from RA patients appeared to grow slightly faster than the synovial cells from OA patients, which is statistically significant ($P < 0.05$) (Fig. 4A).

To examine if this phenomenon is reflected in the signal transduction machinery of synovial cells, we investigated the activation of the EGFR signaling pathway in the AREG-treated and untreated RA synoviocytes. We first examined the phosphorylation of the extracellular signal-regulated kinases (ERK1/2) at Thr202 and Tyr204 by western blot analysis. ERK1/2 phosphorylation indicates the activation of the EGFR signaling pathway.[32] As shown in Fig. 5A, the phosphorylated ERK1/2 bands in the RA synoviocytes showed an increase in intensity when the cells had been treated with AREG; this effect peaked 8–12 h after AREG treatment but continued for 2–3 days. In contrast, the ERK1/2 protein levels remained largely unaffected by AREG treatment.